

# Adaptive aberration correction in confocal scanning fluorescence microscopy

Zhibin Wang (王志斌)<sup>1,3\*</sup>, Guohua Shi (史国华)<sup>1,2</sup>, and Yudong Zhang (张雨东)<sup>1,2</sup>

<sup>1</sup>The Key Laboratory on Adaptive Optics, Chinese Academy of Sciences, Chengdu 610209, China

<sup>2</sup>The Laboratory on Adaptive Optics, Institute of Optics and Electronics, Chinese Academy of Sciences, Chengdu 610209, China

<sup>3</sup>Graduate School of Chinese Academy of Sciences, Beijing 100039, China

\*Corresponding author: zbwang16@gmail.com

Received August 05, 2013; accepted October 23, 2013; posted online March 25, 2014

Adaptive optics is implemented in a confocal scanning fluorescence microscopy using a wavefront sensorless correction scheme. Using the image sharpness as the optimization metric, aberration correction is performed to compensate both system- and specimen-induced aberrations by using stochastic parallel gradient descent algorithm based upon Zernike polynomial modes. We demonstrate the idea of using phantom fluorescence samples experimentally. Enhanced imaging contrast and improved signal level are achieved.

OCIS codes: 110.0110, 180.0180, 170.0170.

doi: 10.3788/COL201412.S11103.

Confocal fluorescence microscope is widely used in biological research, primarily because of its ability to optically ‘section’ thick specimens; the obtained thin imaging slices can then be used to reconstruct three-dimensional images, a capability which is particularly useful in biological applications. However, it is well-known that the resolution and optical sectioning ability can be severely degraded by system- or specimen-induced aberrations. The sources of aberrations are from both the microscopic system and the specimen. The specimen itself brings intrinsic optical aberration due to inhomogeneous optical index of refraction, and the aberration intends to get larger with a deeper imaging depth. The combination of high numeric aperture objective, objective immersion media, cover glass and imaging target degrades beam quality significantly due to different optical refractive indices in each media.

The techniques of adaptive optics (AO), which have been widely used in astronomy and ophthalmology to measure and correct the aberrations caused by atmospheric turbulence and human eye, offer a nearly diffraction-limited resolution. AO has also been combined with confocal scanning laser ophthalmoscope<sup>[1]</sup> to image the living human retina at the single-cell level. In the field of microscopy, several groups have conducted research on wavefront correction related to single-photon or multi-photon scanning microscopy for imaging<sup>[2-4]</sup>.

Conventional AO systems employ a sensor to measure wavefront errors in the image path of the optical system. These measured wavefront errors can be used as feedback for the wavefront corrector in a closed control loop that compensates for aberrations. However, these methods require a point-like reference source, such as the distant guide star used in astronomical systems, to

produce a well-defined wavefront. In adaptive microscopy, the situation is more complicated, as the three-dimensional structure of the specimen shows that the reference source is generally not a point-like source. In effect, the wavefront sensor would receive a multitude of wavefronts, each emanating from different parts of the specimen. Therefore, direct wavefront sensing is not straightforward in microscopy.

Most of the adaptive microscope systems so far used indirect methods of aberration measurement. In general, this indirect approach involves maximization of the photodetector signal using an appropriate optimization scheme. Several of these implementations have used stochastic methods based upon genetic algorithm or hill-climbing algorithm<sup>[5]</sup>. These methods require a large number of iterations that might not be practical for some of the applications where high speed or low exposure is required. Model-based approaches based upon modal wavefront sensing have shown better performance, requiring fewer measurements than model-free methods<sup>[2,6]</sup>, but it requires taking different sets of functions as the predetermined bias functions for aberrations of various magnitudes. The stochastic parallel gradient descent algorithms (SPGD) proposed by Vorontsov<sup>[7]</sup> have been used in other areas of AO and verified to be the fastest search methods. ‘Considering the range of algorithm application and correction speed, we choose SPGD algorithm, which has robust convergence characteristics for different aberrations and can complete the aberration correction in seconds in our microscopy.

We demonstrated an adaptive optics confocal fluorescence scanning laser microscope. ‘A deformable mirror (DM) is used as wavefront corrector to compensate system- or specimen-included aberration. The SPGD

algorithm is used to control the DM. The experimental results showed that the aberration of microscope cannot be neglected and image quality is improved with AO. The optimization algorithm is still effective with more serious aberrations common in deep tissue imaging<sup>7</sup>.

The SPGD algorithm maximizes or minimizes a metric signal corresponding to system performance in an iterative control loop based on randomized perturbations of the system's controllable inputs. The control loop for AO includes temporary changing of the mirror shape by applying perturbations on its independent control inputs (e.g., DM actuators), assessing the effect of these perturbations on the metric (e.g., fluorescence intensity), estimating a metric gradient with respect to control input perturbations, and finally updating the mirror shape to a state that should incrementally increase the metric.

The performance of SPGD algorithm for AO in an actual fluorescence microscopy experiment in deep-tissue imaging is the best when the control basis was Zernike polynomials, with perturbations applied as changes in the Zernike polynomial coefficients.

The aberration in pupil could be expanded as

$$\Phi(u, v) = \sum a_i Z_i(u, v), \quad (1)$$

where,  $Z_i(u, v)$  is the  $i$ -th Zernike polynomial with coefficient  $a_i$ .

The SPGD algorithm could be represented as

$$a_i^{n+1} = a_i^n + k\delta_i^n (J^{n+} - J^{n-}), \quad (2)$$

where,  $\delta_i^n$  is randomized perturbation applied for  $i$ -th control channel, coefficient of  $i$ -th Zernike polynomial, in a direction that is randomly signed;  $J^{n+}$  is the metric when randomized perturbations ( $\delta_1^n, \delta_2^n \dots \delta_i^n, \delta_{i+1}^n \dots$ ) are applied for all control channels;  $J^{n-}$  is the metric when the control channels are perturbed in the opposite direction.

Image sharpness, robust for the design of a sample-independent aberration correction scheme, was chosen as metric of image quality, as aberration could be considered constant in the field of view of microscopy<sup>[4,8]</sup>. Image sharpness is defined as

$$M_{img} = \sum \sum [I_{m,n} - \bar{I}]^2, \quad (3)$$

where  $\bar{I}$  is average gray value of the image.

The first 18 Zernike polynomials are used for aberration correction in this paper and are shown in Fig. 1(b). Tip, tilt and defocus components are removed from the basis modes because they do not affect image quality but change imaging position.

Figure 1(a) shows a schematic of the adaptive microscope. The beam light emitted from a 638 nm laser diode, which has output power about 30 mW, is collimated. The expanded beam is imaged onto a DM (37 actuators). The beam was steered by two scanning mirrors that were imaged onto the pupil plane of the microscope objective. The fluorescence emission was collected

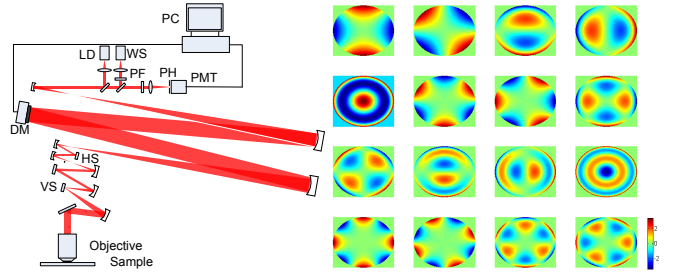


Fig. 1. (a) Schematic diagram of the microscopy and (b) plots of the Zernike basis modes after removal of the displacement mode components.

by an objective lens (Olympus UA water immersion, 40 $\times$ , NA = 0.80). A band-pass filter (Semrock, FF01-670/30 nm) is placed (PH) before the photomultiplier tubes (PMT, Hamamatsu, H7422-20) to filter illumination light. The pinhole used in this microscopy is 50  $\mu$ m. Finally, the fluorescence from the specimen is detected by PMT. Specimen scanning was enabled in the axial  $z$  direction by a motorized translation stage attached to the sample stage. A Hartmann wavefront sensor is used for system calibration and calibration of Zernike basis modes<sup>[9]</sup>. Imaging speed of the microscope is 30 Hz.

In the experiment, we chose a phantom fluorescence sample coated with fluorescent lipophilic tracers DiD (Molecular Probes) fluorescent dye as specimen. Images of specimen with AO off and on are shown in Figs. 2(a) and (c), respectively. The metric value curve of images during aberration correction process is shown in Fig. 2(e). After 170 iterations, the metric of image increase by 43%. As the specimen is a two-dimensional planar structure, we could measure aberration of fluorescence using the Hartmann wavefront sensor. Aberration of the microscopy was measured by Hartmann sensor and is shown in Fig. 2(b), root mean square (RMS) of system aberration is 0.142  $\mu$ m. After aberration correction with SPGD algorithm, RMS reduces to 0.079  $\mu$ m. By comparing the coefficients of Zernike polynomials, as shown in Fig. 2(f), it is understood that most of the Zernike components of system aberration are compensated except the eighth-order and eighteenth-order Zernike components. It is mainly due to the DM fitting error of these components.

Then, an additional random aberration with RMS 0.4  $\mu$ m was introduced into the system. The random aberration and system aberration were measured by Hartmann wavefront sensor [Fig. 3(b)], with RMS 0.532  $\mu$ m. Fluorescence image of the specimen was severely degraded as shown in Fig. 3(a). After 250 SPGD iterations, sharpness of the image increases eight-fold. The metric value curve of images during aberration correction process is shown in Fig. 3(e).

After aberration correction with SPGD algorithm, RMS reduces to 0.095  $\mu$ m. The comparison of coefficients of Zernike polynomials is shown in Fig. 3(f) and most of the Zernike components of aberration are corrected.

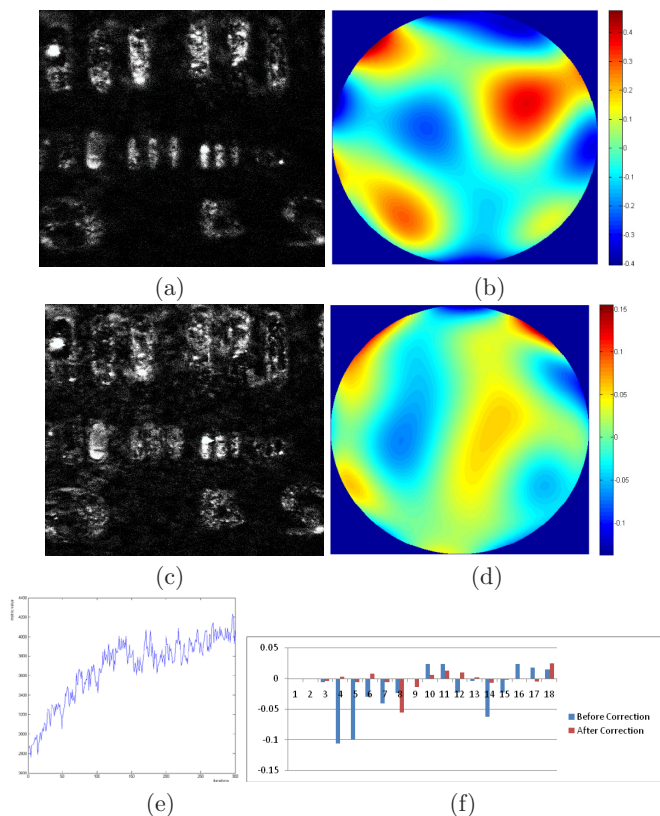


Fig. 2. (a) Fluorescence image with AO off; (b) wavefront measured by Hartmann sensor before correcting system aberration; (c) fluorescence image with AO on; (d) wavefront measured by Hartmann sensor after correcting system aberration; (e) metric value of images during aberration correction process; and (f) coefficients of the Zernike polynomials used for aberration correction.

The aberration-corrected images obtained with the microscope show enhanced contrast and improvement of fluorescence intensity. The AO could be widely beneficial in the field of confocal microscopy that suffers from the detrimental effects of system- and specimen-induced aberrations. The results also show that the eighth-order and eighteenth-order Zernike components are not corrected effectively. It is mainly due to the DM fitting error of these components, which will be next focus of our work.

It needs 6–9 s to accomplish aberration correction mainly limited by imaging speed of microscope and convergence rate of SPGD algorithm. Improving SPGD algorithm or combining it with other optimization algorithms such as modal algorithm may be a possible solution to accelerate the process of aberration correction.

In conclusion, we demonstrate that stochastic parallel gradient descent AO is effective in correcting aberration in confocal microscopy. Zernike basis is used to characterize aberration source and as control basis of SPGD algorithms. The fluorescence images with aberration correction show enhanced contrast and improvement in fluorescence intensity.

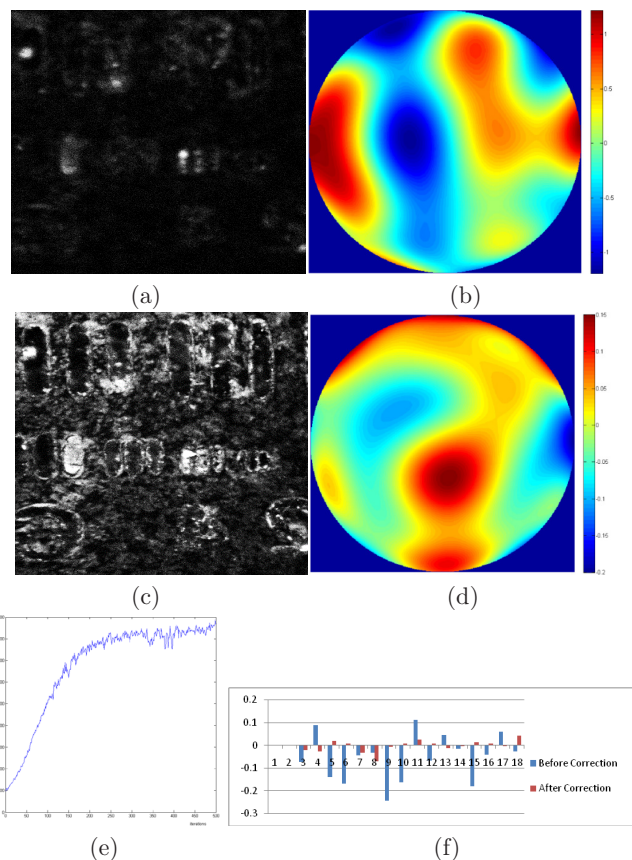


Fig. 3. (a) Fluorescence image of specimen with a random aberration; (b) wavefront measured by Hartmann sensor before correcting random aberration; (c) fluorescence image of the specimen after aberration correction; (d) wavefront measured by Hartmann sensor after correcting random aberration; (e) metric value of images during aberration correction process; and (f) coefficients of the Zernike polynomials used for aberration correction.

This work was supported by the National Major Scientific Equipment program (No. 2012YQ120080), the National Science Foundation of China (No. 61108082), the Sichuan Youth Science & Technology Foundation (No. 2013JQ0028), and the West Light Foundation of the Chinese Academy of Sciences.

## References

1. L. Jing, L. Hao, W. Ling, S. Guohua, and Z. Yudong, Proc. SPIE **7519**, 75191I (2009).
2. Y. Zhou, T. Bifanoand, and C. Lin, Proc. SPIE **7931**, 79310H (2011)
3. M. J. Booth, M. A. A. Neil, R. Juskaitis, and T. Wilson, Proc. Natl Acad. Sci. **99**, 5788 (2002).
4. N. Ji, T. R. Sato, and E. Betzig, Proc. Natl Acad. Sci. **109**, 22 (2011).
5. W. Lubeigt, S. P. Poland, G. J. Valentine, A. J. Wright, J. M. Girkin, and D. Burns, Appl. Opt. **49**, 307 (2010).
6. M. J. Booth, Opt. Lett. **32**, 5 (2007).
7. M. A. Vorontsov, G. W. Carhart, M. Cohen, and G. Cauwenberghs, J. Opt. Soc. Am. A **17**, 1440 (2000).
8. D. Débarre, E. J. Botcherby, T. Watanabe, S. Srinivas, M. J. Booth, and T. Wilson, Opt. Lett. **34**, 2495 (2009).
9. A. Thayil and M. J. Booth, J. Eur. Opt. Soc. **6**, 11045 (2011).